PERGAMON

International Journal of Solids and Structures 38 (2001) 8735–8752

INTERNATIONAL JOURNAL OF SOLIDS and STRUCTURES

www.elsevier.com/locate/ijsolstr

FEM modeling of adaptive composite structures using a reduced higher-order plate theory via penalty functions

H. Fukunaga [a], N. Hu [a,*], G.X. Ren [b]

[a] *Department of Aeronautics and Space Engineering, Tohoku University, 01 Aramaki-Aoba, Aoba-ku, Sendai 980-8579, Japan*
[b] *Department of Engineering Mechanics, Tsinghua University, Beijing 100084, China*

Received 5 September 2000; in revised form 23 March 2001

Abstract

This paper presents a finite element model for analyzing the composite laminates containing the piezoelectrics statistically or dynamically. First, to model the moderately thick laminated plates, a simple higher-order plate theory, which can satisfy the free conditions of transverse shear strains on the top and bottom surfaces of plates, have been adopted. To set up a C^0-type FEM scheme, two artificial variables in the displacement field have been introduced to avoid the higher-order derivatives from the higher-order plate theory. The corresponding constraint conditions from two artificial variables have been enforced effectively through the penalty function method using the reduced integral scheme within the element area. Second, a generalized coupling FEM model for the mechanical and electric fields from the variational framework have been proposed. Finally, various examples studied in many previous researches have been employed to verify the justification, accuracy and efficiency of the present model.

Keywords: Adaptive structures; Composite laminates; Piezoelectrics; C^0-type finite element; Higher-order plate theory

1. Introduction

The development of a new class of "smart" composite materials and adaptive structures with sensory/active capabilities may further improve the performance and reliability of aeronautical structural systems. Such materials can combine the superior mechanical properties of composite materials, as well as incorporate the additional inherent capability to sense and adapt their static and dynamic response. Until now, there have been many theories and models for analyzing composite laminates containing active and passive piezoelectric layers. One approach, which uses simplifying approximations attempting to replicate the "induced strain" or electric fields generated by a piezoelectric layer under an external electric field or applied load (see, Crawley and Lazarus, 1989; Tzou and Tseng, 1990; Keilers and Chang, 1995; Chattopadhyay and Seeley, 1997; Seeley and Chattopadhyay, 1999). However, through an exact solution for

* Corresponding author. Tel.: +81-22-217-4109; fax: +81-22-217-6995/6996.
E-mail address: hu@ssl.mech.tohoku.ac.jp (N. Hu).

0020-7683/01/$ - see front matter
PII: S0020-7683(01)00072-5

piezoelectric laminated plates, Heyliger and Saravanos (1995) has pointed out that the electric and elastic field distributions may be poorly modeled using these simplifying theories. Therefore, another approach starting from the variational methods, which can tackle the coupling effects of mechanical and electric fields more efficiently, have also been paid widespread attention (see, Suleman and Venkaya, 1995; Saravanos et al., 1997; Lee and Saravanos, 1997, 2000; Correia et al., 2000; Chee et al., 2000). To model the deformation of laminated plates, the approaches, which based on the classical laminate beam or plate theory (e.g., Crawley and Lazarus, 1989; Keilers and Chang, 1995), have been initially developed. These approaches should be restricted to thin plate applications since the linear strain distribution through the thickness and zero transverse shear stresses are assumed. However, effects of transverse shear stresses are usually important in composite laminates. Furthermore, the stress distributions in structures actuated by piezoelectric materials are known to be quite complex (see, Mollenhauer and Griffen, 1994). Physically, the assumption of a linear strain distribution through the thickness of a substrate material, undergoing induced strain actuation from piezoelectric materials, seems oversimplified, especially for thick plates. As a result, it is necessary to use a shear deformation theory to address moderately thick and thick laminate constructions. The first-order shear deformation theory (e.g., Tzou and Tseng, 1990; Suleman and Venkaya, 1995; Tzou and Ye, 1996) has been used for modeling the laminates with piezoelectric actuation using the FEM. Furthermore, the layerwise theory (see, e.g., Robbins and Reddy, 1991; Saravanos et al., 1997; Lee and Saravanos, 1997, 2000) and a three-dimensional (3D) coupled-analysis model (e.g., Ha et al. (1992) in FEM and Bisegna and Maceri (1996) in closed form theoretical solutions) have also been advocated. Kim et al. (1997) also proposed a numerical model, in which 3D brick elements are employed for piezoelectrics and flat-shell elements for structures. For these approaches, the more accurate representation of piezoelectric actuation and transverse shear stress distribution can be obtained. For instance, Robbins and Reddy (1991) and Saravanos et al. (1997) have shown the differences between the classical theory and the more sophisticated, but computationally expensive layerwise theory.

To model the moderate thick composites with surface bonded or embedded actuators, it is important to have a more effective general theory for accurately evaluating the effects of normal and transverse shear stresses on actuator or sensor performance. It has long been recognized that higher-order laminate theories may provide an effective solution tool for accurately predicting the deformation behavior of composite laminates subjected to bending loads. Some recent researches (see, e.g., Chattopadhyay and Seeley, 1997; Seeley and Chattopadhyay, 1999; Gaudenzi, 1998; Correia et al., 2000; Chee et al., 2000) have applied the various higher-order theories to model the laminated plates with piezoelectrics. For instance, Gaudenzi (1998) used a simple higher-order beam theory and solved the pure bending problem of a beam under membrane actuation in a closed form. Furthermore, Correia et al. (2000) and Chee et al. (2000) used the higher-order theory (Lo et al., 1977) in their FEM models, which considered the transverse normal strain. They have also shown the insufficiency of the first-order shear deformation theory in the adaptive structural modeling. In this higher-order plate theory, there are full third-order expressions for the in-plane displacements and a full second-order expression for the transverse displacement. Consequently, the free conditions of transverse shear stresses at the free plate surfaces cannot usually be guaranteed and the resulted FEM models possess high nodal degrees of freedom. Hence, the computational amounts are comparatively high in these models. Chattopadhyay and Seeley (1997) and Seeley and Chattopadhyay (1999) employed a simple higher-order plate theory by Vlasov (1957) and Reddy (1984). In this theory, the consistent displacement field can accurately satisfies the free boundary conditions of transverse shear strains at the free surfaces while maintaining continuity of transverse shear strains through the thickness. The developed FEM model possesses a reasonable amount of computational effort compared to classical or first-order shear deformation theory. However, a non-conforming element technique only suitable for elements of the rectangular shape was employed. This element cannot pass in the constant strain patch test for the irregular shaped elements. It is well known that the common FEM models based on the piecewise continuity perform poorly in the computation of derivatives, especially higher-order derivatives. To obtain

stable results, the C^0-type elements are generally desirable. Furthermore, the so-called "induced strain" simplifying approach was employed in their researches by neglecting the coupling effects of mechanical and electric fields.

In this paper, to model the moderately thick composite laminates containing piezoelectrics, a C^0-type element based on the simple higher-order theory by Vlasov (1957) and Reddy (1984) has been developed. It should be noted that the displacement field in this theory was derived for non-piezoelectric materials based on zero transverse strains in the top and bottom surfaces. For structures where the piezoelectrics materials may be on the top and bottom surfaces, due to the coupled constitutive equations, these zero transverse shear strains do not imply zero transverse shear stresses. Also, the variational framework, which couples the influences of the mechanical and electric fields, has been adopted for better predicting the response of sensors. Furthermore, various verifications from the previous researches for the present model have been carried out.

2. Theory

2.1. Kinematics and constitutive relationships

As stated previously, a simple higher-order plate theory has been adopted here. The third-order displacement fields in this theory can be found from Reddy's work (1984), which are cited as follows:

$$u(x,y,z) = u_0 + z\left[\theta_x - \frac{4}{3}\left(\frac{z}{h}\right)^2\left(\theta_x + \frac{\partial w}{\partial x}\right)\right] \tag{1a}$$

$$v(x,y,z) = v_0 + z\left[\theta_y - \frac{4}{3}\left(\frac{z}{h}\right)^2\left(\theta_y + \frac{\partial w}{\partial y}\right)\right] \tag{1b}$$

$$w(x,y) = w_0 \tag{1c}$$

where u_0, v_0 and w_0 are the displacements on the mid-plane plane, and θ_x and θ_y the rotations due to shear deformation about the y and x axes, respectively.

Since the transverse normal stress is of the order (h/a^2) times the in-plane normal stresses, the assumption that $w(x,y)$ is not a function of the thickness coordinates is justified. The above displacement fields can be derived from a complete third-order expansion of the displacement field using free conditions of the transverse strains on the top and bottom surfaces of plate, i.e., $\varepsilon_{xz}(x,y,\pm(h/2)) = 0$ and $\varepsilon_{yz}(x,y,\pm(h/2)) = 0$. Vlasov (1957) and Jemielita (1975) are the first ones to derive the above third-order theories. Some other researchers, such as Murthy (1981) and Reddy (1984), applied the above theory into the laminated composite plates. Reddy (1984) is the first one to derive variationally consistent third-order theory for composite laminates.

Under the above displacement field description, the strains associated with the displacements in Eqs. (1a)–(1c) can be described as follows:

$$\varepsilon_x(x,y,z) = \varepsilon_x^0 + z(\kappa_x^0 + z^2\kappa_x^1) \tag{2a}$$

$$\varepsilon_y(x,y,z) = \varepsilon_y^0 + z(\kappa_y^0 + z^2\kappa_y^1) \tag{2b}$$

$$\varepsilon_{xy}(x,y,z) = \varepsilon_{xy}^0 + z(\kappa_{xy}^0 + z^2\kappa_{xy}^1) \tag{2c}$$

$$\varepsilon_z(x,y,z) = 0 \tag{2d}$$

$$\varepsilon_{yz}(x,y,z) = \varepsilon^0_{yz} + z^2\kappa^1_{yz} \tag{2e}$$

$$\varepsilon_{xz}(x,y,z) = \varepsilon^0_{xz} + z^2\kappa^1_{xz} \tag{2f}$$

where

$$\varepsilon^0_x = \frac{\partial u_0}{\partial x}, \quad \varepsilon^0_y = \frac{\partial v_0}{\partial y} \tag{3a}$$

$$\varepsilon^0_{xy} = \frac{\partial u_0}{\partial y} + \frac{\partial v_0}{\partial x} \tag{3b}$$

$$\kappa^0_x = \frac{\partial \theta_x}{\partial x}, \quad \kappa^0_y = \frac{\partial \theta_y}{\partial y} \tag{3c}$$

$$\kappa^0_{xy} = \frac{\partial \theta_x}{\partial y} + \frac{\partial \theta_y}{\partial x} \tag{3d}$$

$$\kappa^1_x = -\frac{4}{3h^2}\left(\frac{\partial \theta_x}{\partial x} + \frac{\partial^2 w}{\partial x^2}\right), \qquad \kappa^1_y = -\frac{4}{3h^2}\left(\frac{\partial \theta_y}{\partial y} + \frac{\partial^2 w}{\partial y^2}\right) \tag{3e}$$

$$\kappa^1_{xy} = -\frac{4}{3h^2}\left(\frac{\partial \theta_x}{\partial y} + \frac{\partial \theta_y}{\partial x} + 2\frac{\partial^2 w}{\partial x \partial y}\right) \tag{3f}$$

$$\varepsilon^0_{xz} = \theta_x + \frac{\partial w}{\partial x}, \qquad \varepsilon^0_{yz} = \theta_y + \frac{\partial w}{\partial y} \tag{3g}$$

$$\kappa^1_{xz} = -\frac{4}{h^2}\left(\theta_x + \frac{\partial w}{\partial x}\right), \qquad \kappa^1_{yz} = -\frac{4}{h^2}\left(\theta_y + \frac{\partial w}{\partial y}\right) \tag{3h}$$

The linear piezoelectric constitutive equations coupling the elastic field and the electric field, can be written as

$$\boldsymbol{\sigma} = \overline{\mathbf{Q}}\boldsymbol{\varepsilon} - \overline{\mathbf{e}}\mathbf{E} \tag{4a}$$

$$\mathbf{D} = \overline{\mathbf{e}}^{\mathrm{T}}\boldsymbol{\varepsilon} + \mathbf{p}\mathbf{E} \tag{4b}$$

where $\boldsymbol{\sigma} = \{\sigma_x, \sigma_y, \sigma_{xy}, \sigma_{yz}, \sigma_{xz}\}^{\mathrm{T}}$ is the elastic stress vector and $\boldsymbol{\varepsilon} = \{\varepsilon_x, \varepsilon_y, \varepsilon_{xy}, \varepsilon_{yz}, \varepsilon_{xz}\}^{\mathrm{T}}$ the elastic strain vector as stated above. $\overline{\mathbf{Q}}$ the elastic constitutive matrix in the laminate (x,y,z) coordinate system, $\overline{\mathbf{e}}$ the piezoelectric stress coefficients matrix in the same coordinate system, $\mathbf{E}$ the electric field vector, $\mathbf{D}$ the electric displacement vector and $\mathbf{p}$ is the dielectric matrix.

The stresses for an arbitrary ply k, written in the laminate (x,y,z) coordinate system are evaluated by

$$\boldsymbol{\sigma}_k = \overline{\mathbf{Q}}_k\boldsymbol{\varepsilon}_k - \overline{\mathbf{e}}_k\mathbf{E}_k \tag{5}$$

In this research, due to no consideration of ε_z, $\overline{\mathbf{Q}}_k$ matrix can be described as follows

$$\overline{\mathbf{Q}}_k = \begin{bmatrix} \overline{Q}^k_{11} & \overline{Q}^k_{12} & \overline{Q}^k_{16} & 0 & 0 \\ \overline{Q}^k_{12} & \overline{Q}^k_{22} & \overline{Q}^k_{26} & 0 & 0 \\ \overline{Q}^k_{16} & \overline{Q}^k_{26} & \overline{Q}^k_{66} & 0 & 0 \\ 0 & 0 & 0 & \overline{Q}^k_{44} & \overline{Q}^k_{45} \\ 0 & 0 & 0 & \overline{Q}^k_{45} & \overline{Q}^k_{55} \end{bmatrix} = \begin{bmatrix} \overline{\mathbf{Q}}^p_k & \mathbf{0} \\ \mathbf{0} & \overline{\mathbf{Q}}^s_k \end{bmatrix} \tag{6}$$

The piezoelectric coefficient matrix $\overline{\mathbf{e}}_k$ is expressed as

$$\overline{\mathbf{e}}_k = \begin{bmatrix} 0 & 0 & \overline{e}^k_{31} \\ 0 & 0 & \overline{e}^k_{32} \\ 0 & 0 & \overline{e}^k_{36} \\ 0 & 0 & 0 \\ 0 & 0 & 0 \end{bmatrix} \tag{7}$$

The electric field vector $\mathbf{E}_k$ in the kth ply is the negative gradient of the electric potential, i.e.

$$\mathbf{E}_k = -\nabla\phi_k = \{0, 0, E^z_k\}^{\mathrm{T}} \tag{8}$$

where it is assumed that the electric field is applied through the thickness direction and E^z_k is the electric field in the thickness direction, which can be written as

$$E^z_k = -\phi_k / t_k \tag{9}$$

where ϕ_k is the electric voltage applied across the kth layer and t_k is the thickness of the kth layer.

Eq. (5) can also be expressed as

$$\boldsymbol{\sigma}_k = \overline{\mathbf{Q}}_k(\boldsymbol{\varepsilon}_k - \overline{\mathbf{d}}_k \mathbf{E}_k) \tag{10}$$

where $\overline{\mathbf{d}}_k$ is the piezoelectric strain coefficient matrix in the (x, y, z) coordinate system, for the kth layer, related with $\overline{\mathbf{e}}_k$ by

$$\overline{\mathbf{e}}_k = \overline{\mathbf{Q}}_k \overline{\mathbf{d}}_k \tag{11}$$

The dielectric matrix $\mathbf{p}$ is chosen here as

$$\mathbf{p} = \begin{bmatrix} 0 & 0 & 0 \\ 0 & 0 & 0 \\ 0 & 0 & p_{33} \end{bmatrix} \tag{12}$$

where p_{33} is the electrical permittivity.

2.2. Finite element implementation

The second-order derivatives of displacement appear in the strain–displacement relationships, implying that displacement-based elements of C^1-continuity are generally necessary in the finite element procedure. To derive a weak form of the principle of virtual work suitable for finite element implementation using C^0-shape functions, a strategy has been proposed here to introduce additional nodal degrees of freedom and to enforce the kinematics constraints by penalty parameters.

Introduce a vector $\boldsymbol{\chi}$ as follows

$$\boldsymbol{\chi} = \{\chi_x, \chi_y\}^{\mathrm{T}} = \left\{ \frac{\partial w}{\partial x}, \frac{\partial w}{\partial y} \right\}^{\mathrm{T}} \tag{13}$$

Then, the higher-order curvature and transverse shear terms in Eqs. (3a)–(3h) become as

$$\kappa_x^1 = -\frac{4}{3h^2}\left(\frac{\partial\theta_x}{\partial x} + \frac{\partial\chi_x}{\partial x}\right), \qquad \kappa_y^1 = -\frac{4}{3h^2}\left(\frac{\partial\theta_y}{\partial y} + \frac{\partial\chi_y}{\partial y}\right) \tag{14a}$$

$$\kappa_{xy}^1 = -\frac{4}{3h^2}\left(\frac{\partial\theta_x}{\partial y} + \frac{\partial\theta_y}{\partial x} + \frac{\partial\chi_x}{\partial y} + \frac{\partial\chi_y}{\partial x}\right) \tag{14b}$$

$$\varepsilon_{xz}^0 = \theta_x + \chi_x, \qquad \varepsilon_{yz}^0 = \theta_y + \chi_y \tag{14c}$$

$$\kappa_{xz}^1 = -\frac{4}{h^2}(\theta_x + \chi_x), \qquad \kappa_{yz}^1 = -\frac{4}{h^2}(\theta_y + \chi_y) \tag{14d}$$

The constraint conditions $\psi_x = \chi_x - (\partial w/\partial x) = 0$ and $\psi_y = \chi_y - (\partial w/\partial y) = 0$ will be tackled in the principle of virtual work through the penalty function method.

This technique is of generality for dealing with the higher-order derivatives in some special problems. For example, in the strain gradient problem, which caused the interests of many researchers, there are usually second-order derivatives in most of strain gradient theories, such as those starting from the pioneering Coesserat couple stress theory or Toupin–Mindlin theory. Then, the usual C^1-type FEM schemes have been adopted widely. Unfortunately, till now, no robust C^1-continuous elements are available in the present literature, and their performances are usually poor in such as delivering the accurate pressure distribution for incompressible and non-linear solids or describing the shear strains at the crack front for Model II crack problems (Shu et al., 1999). Actually, the present idea can be employed in this kind of field when higher-order derivatives appear. Now, the nodal displacement vector is $\mathbf{u}_i^e = \{u_0^i, v_0^i, w_0^i, \theta_x^i, \theta_y^i, \chi_x^i, \chi_y^i\}^{\mathrm{T}}$, i.e. the 7 degrees of freedom on one node, which are the same with that in the FEM model (Chattopadhyay and Seeley, 1997; Seeley and Chattopadhyay, 1999), but lower than those in the models (Correia et al., 2000; Chee et al., 2000).

Then, the mechanical and electrical response of piezoelectrics can be obtained through applying the principle of virtual work to the equation of balance of momentum in the elastic field and the Maxwell's equation $D_{i,i} = 0$ in the electric field. For an arbitrary element of volume V_e, the modified principle of the virtual work due to introduction of the constraint conditions can be described as

$$\int_{V_e} (\delta\boldsymbol{\varepsilon}^{\mathrm{T}}\overline{\mathbf{Q}}\boldsymbol{\varepsilon} - \delta\boldsymbol{\varepsilon}^{\mathrm{T}}\overline{\mathbf{e}}\mathbf{E} - \delta\mathbf{E}^{\mathrm{T}}\overline{\mathbf{e}}^{\mathrm{T}}\boldsymbol{\varepsilon} - \delta\mathbf{E}^{\mathrm{T}}\mathbf{p}\mathbf{E} + \delta\boldsymbol{\psi}^{\mathrm{T}}\mathbf{D}_{\mathrm{p}}\boldsymbol{\psi} + \rho\,\delta\mathbf{u}^{\mathrm{T}}\ddot{\mathbf{u}})\,\mathrm{d}V - \delta W_u + \delta W_\phi = 0 \tag{15}$$

where $\boldsymbol{\psi} = \{\psi_x, \psi_y\}^{\mathrm{T}}$ and $\mathbf{D}_{\mathrm{p}}$ is the penalty matrix, which can be expressed as

$$\mathbf{D}_{\mathrm{p}} = \begin{bmatrix} \alpha_x & 0 \\ 0 & \alpha_y \end{bmatrix} \tag{16}$$

The choice of penalty parameters α_x and α_y will be discussed later.

It can found that there is no second-order derivative in the above principle of virtual work. It is also interesting to note that there is no unknown w occurring in the first four terms of Eq. (15). It exists only in the penalty term. Performing the integral of Eq. (15) through the plate thickness direction, the following equation can be obtained

$$\int_{S_e} \left[\delta\boldsymbol{\varepsilon}^{*\mathrm{T}}\mathbf{D}_{\mathrm{c}}\boldsymbol{\varepsilon}^* - \delta\boldsymbol{\varepsilon}^{*\mathrm{T}}\overline{\mathbf{e}}^*\mathbf{E} - \delta\mathbf{E}^{\mathrm{T}}\overline{\mathbf{e}}^{*\mathrm{T}}\boldsymbol{\varepsilon}^* - \int_{-h/2}^{h/2}(\delta\mathbf{E}^{\mathrm{T}}\mathbf{p}\mathbf{E})\,\mathrm{d}z + \int_{-h/2}^{h/2}(\delta\boldsymbol{\psi}^{\mathrm{T}}\mathbf{D}_{\mathrm{p}}\boldsymbol{\psi})\,\mathrm{d}z + \int_{-h/2}^{h/2}(\rho\,\delta\mathbf{u}^{\mathrm{T}}\ddot{\mathbf{u}})\,\mathrm{d}z\right]\mathrm{d}S - \delta W_u + \delta W_\phi = 0 \tag{17}$$

where S_e is the element area, h the total thickness of the current element, and the generalized strain vector $\boldsymbol{\varepsilon}^*$ can be expressed as

$$\boldsymbol{\varepsilon}^* = \{\boldsymbol{\varepsilon}^0, \boldsymbol{\kappa}^0, \boldsymbol{\kappa}^1, \boldsymbol{\varepsilon}_s^0, \boldsymbol{\kappa}_s^1\} \tag{18}$$

where

$$\boldsymbol{\varepsilon}^0 = \{\varepsilon_x^0, \varepsilon_y^0, \varepsilon_{xy}^0\}^T \tag{19a}$$

$$\boldsymbol{\kappa}^0 = \{\kappa_x^0, \kappa_y^0, \kappa_{xy}^0\}^T, \qquad \boldsymbol{\kappa}^1 = \{\kappa_x^1, \kappa_y^1, \kappa_{xy}^1\}^T \tag{19b}$$

$$\boldsymbol{\varepsilon}_s^0 = \{\varepsilon_{yz}^0, \varepsilon_{xz}^0\}^T, \qquad \boldsymbol{\kappa}_s^1 = \{\kappa_{yz}^1, \kappa_{xz}^1\}^T \tag{19c}$$

For the nodal displacement vector $\mathbf{u}_i^e = \{u_0^i, v_0^i, w_0^i, \theta_x^i, \theta_y^i, \chi_x^i, \chi_y^i\}^T$ at the ith node, the strain–displacement matrix $\mathbf{B}_d^i$ for the generalized strain vector can be expressed as

$$\mathbf{B}_d^i = \begin{bmatrix}
\partial N_i/\partial x & 0 & 0 & 0 & 0 & 0 & 0 \\
0 & \partial N_i/\partial y & 0 & 0 & 0 & 0 & 0 \\
\partial N_i/\partial y & \partial N_i/\partial x & 0 & 0 & 0 & 0 & 0 \\
0 & 0 & 0 & \partial N_i/\partial x & 0 & 0 & 0 \\
0 & 0 & 0 & 0 & \partial N_i/\partial y & 0 & 0 \\
0 & 0 & 0 & \partial N_i/\partial y & \partial N_i/\partial x & 0 & 0 \\
0 & 0 & 0 & (c/3)(\partial N_i/\partial x) & 0 & (c/3)(\partial N_i/\partial x) & 0 \\
0 & 0 & 0 & 0 & (c/3)(\partial N_i/\partial y) & 0 & (c/3)(\partial N_i/\partial y) \\
0 & 0 & 0 & (c/3)(\partial N_i/\partial y) & (c/3)(\partial N_i/\partial x) & (c/3)(\partial N_i/\partial y) & (c/3)(\partial N_i/\partial x) \\
0 & 0 & 0 & N_i & 0 & N_i & 0 \\
0 & 0 & 0 & 0 & N_i & 0 & N_i \\
0 & 0 & 0 & cN_i & 0 & cN_i & 0 \\
0 & 0 & 0 & 0 & cN_i & 0 & cN_i
\end{bmatrix} \tag{20}$$

where c is a constant, i.e. $-4/h^2$. The final strain–displacement matrix is expressed as

$$\mathbf{B}_d = [\mathbf{B}_d^1, \ldots, \mathbf{B}_d^i, \ldots, \mathbf{B}_d^{nd}] \tag{21}$$

where nd is the number of nodes in one element.

In the Mindlin type element, the transverse shear terms like those in Eq. (3g), and the strain–displacement matrix for the nodal displacements $\mathbf{u}_i^e = \{u_0^i, v_0^i, w_0^i, \theta_x^i, \theta_y^i\}^T$ is

$$\mathbf{B}_{MS} = \begin{bmatrix} 0 & 0 & \partial N_i/\partial x & N_i & 0 \\ 0 & 0 & \partial N_i/\partial y & 0 & N_i \end{bmatrix} \tag{22}$$

For thin plate situation the transverse shear strains should tend towards zero, and the shear strain energy terms play a role of penalty functions to force this conditions to be satisfied. If the full integration is carried out, due to the different orders of functions (i.e. unmatching) in the two entries of one row in Eq. (22), these penalty conditions cannot be exactly satisfied numerically, which leads to the overstiff results, i.e. the so-called "locking" phenomenon. Generally, it is overcome using the reduced integration scheme. However, by noting the 10th and 11th rows for the transverse shear strains in Eq. (20), unlike the Mindlin plate element, there is no derivative in the transverse shear terms. The orders of the interpolation functions are identical and no unmatching appears when performing the full Gauss integration scheme. A merit of the present technique is that the accurate integration for the energy due to transverse shear terms can be obtained, and the reduced Gauss integration is unnecessary at this stage.

Further, the material matrix $\mathbf{D}_c$, which related the generalized strain components with the generalized stress resultants, can be described as

$$\begin{Bmatrix} \mathbf{N} \\ \mathbf{M} \\ \mathbf{P} \\ \mathbf{Q} \\ \mathbf{R} \end{Bmatrix} = \mathbf{D}_c\boldsymbol{\varepsilon}^* = \begin{bmatrix} \mathbf{A} & \mathbf{B} & \mathbf{G} & \mathbf{0} & \mathbf{0} \\ \mathbf{B} & \mathbf{D} & \mathbf{F} & \mathbf{0} & \mathbf{0} \\ \mathbf{G} & \mathbf{F} & \mathbf{H} & \mathbf{0} & \mathbf{0} \\ \mathbf{0} & \mathbf{0} & \mathbf{0} & \mathbf{A}_s & \mathbf{B}_s \\ \mathbf{0} & \mathbf{0} & \mathbf{0} & \mathbf{B}_s & \mathbf{D}_s \end{bmatrix} \begin{Bmatrix} \boldsymbol{\varepsilon}^0 \\ \boldsymbol{\kappa}^0 \\ \boldsymbol{\kappa}^1 \\ \boldsymbol{\varepsilon}_s^0 \\ \boldsymbol{\kappa}_s^1 \end{Bmatrix} \tag{23}$$

where the generalized stress components are: $\mathbf{N} = \{N_x, N_y, N_{xy}\}^T$, $\mathbf{M} = \{M_x, M_y, M_{xy}\}^T$, $\mathbf{P} = \{P_x, P_y, P_{xy}\}^T$, $\mathbf{Q} = \{Q_{yz}, Q_{xz}\}^T$, $\mathbf{R} = \{R_{yz}, R_{xz}\}^T$, respectively.

The material sub-matrices in Eq. (23) can be obtained from

$$(\mathbf{A}, \mathbf{B}, \mathbf{D}, \mathbf{G}, \mathbf{F}, \mathbf{H}) = \int_{-h/2}^{h/2} \overline{\mathbf{Q}}_k^p (1, z, z^2, z^3, z^4, z^6)\, \mathrm{d}z \tag{24a}$$

$$(\mathbf{A}_s, \mathbf{B}_s, \mathbf{D}_s) = \int_{-h/2}^{h/2} \overline{\mathbf{Q}}_k^s (1, z^2, z^4)\, \mathrm{d}z \tag{24b}$$

Furthermore, the $\overline{\mathbf{e}}^*$ matrix can be expressed as

$$\overline{\mathbf{e}}^* = \{\overline{\mathbf{e}}_1^*, \overline{\mathbf{e}}_2^*, \ldots, \overline{\mathbf{e}}_k^*, \ldots, \overline{\mathbf{e}}_{\mathrm{npl}}^*\} \tag{25}$$

where npl the number of piezoelectric layers within the current element, and the sub-matrix $\overline{\mathbf{e}}_k^*$ can be obtained from

$$\overline{\mathbf{e}}_k^* = \begin{bmatrix} \left(\int_{-h/2}^{h/2} \overline{\mathbf{Q}}_k^p \,\mathrm{d}z\right) \overline{\mathbf{d}}_k \\ \left(\int_{-h/2}^{h/2} \overline{\mathbf{Q}}_k^p z \,\mathrm{d}z\right) \overline{\mathbf{d}}_k \\ \left(\int_{-h/2}^{h/2} \overline{\mathbf{Q}}_k^p z^3 \,\mathrm{d}z\right) \overline{\mathbf{d}}_k \\ \mathbf{0} \\ \mathbf{0} \end{bmatrix} \tag{26}$$

where the above integrals are only performed for the piezoelectric layers. Also, the dimensions of zero matrices $\mathbf{0}$ in Eq. (26) are 2×3, and the $\overline{\mathbf{d}}_k$ matrix is given by

$$\overline{\mathbf{d}}_k = \begin{bmatrix} 0 & 0 & \overline{d}_{31}^k \\ 0 & 0 & \overline{d}_{32}^k \\ 0 & 0 & 0 \end{bmatrix} \tag{27}$$

In the present element, the electric potential within one piezoelectric layer of one element is assumed to be constant in the x–y plane for simplicity (see, Suleman and Venkaya, 1995; Correia et al., 2000), and then $\mathbf{E}$ matrix can be predicted as follows

$$\mathbf{E} = \mathbf{B}_\phi \boldsymbol{\phi}^e \tag{28}$$

where $\mathbf{B}_\phi$ is expressed as

$$\mathbf{B}_\phi = \begin{bmatrix} 0 & 0 & 0 & \cdots & \cdots & \cdots & \cdots & \cdots & \vdots & \vdots & \vdots \\ 0 & 0 & 0 & \cdots & \cdots & \cdots & \cdots & \cdots & \vdots & \vdots & \vdots \\ 0 & 0 & 1/t_1 & \cdots & \cdots & \cdots & \cdots & \cdots & \vdots & \vdots & \vdots \\ \vdots & \vdots & \vdots & \ddots & \cdots & \cdots & \cdots & \cdots & \vdots & \vdots & \vdots \\ \vdots & \vdots & \vdots & \cdots & 0 & 0 & 0 & \cdots & \vdots & \vdots & \vdots \\ \vdots & \vdots & \vdots & \cdots & 0 & 0 & 0 & \cdots & \vdots & \vdots & \vdots \\ \vdots & \vdots & \vdots & \cdots & 0 & 0 & 1/t_k & \cdots & \vdots & \vdots & \vdots \\ \vdots & \vdots & \vdots & \cdots & \cdots & \cdots & \cdots & \ddots & \vdots & \vdots & \vdots \\ \vdots & \vdots & \vdots & \cdots & \cdots & \cdots & \cdots & \cdots & 0 & 0 & 0 \\ \vdots & \vdots & \vdots & \cdots & \cdots & \cdots & \cdots & \cdots & 0 & 0 & 0 \\ \vdots & \vdots & \vdots & \cdots & \cdots & \cdots & \cdots & \cdots & 0 & 0 & 1/t_{\text{npl}} \end{bmatrix} \tag{29}$$

and $\boldsymbol{\phi}^e$ is

$$\boldsymbol{\phi}^e = \{\phi_1, \ldots, \phi_k, \ldots, \phi_{\text{npl}}\}^{\text{T}} \tag{30}$$

Here, as some authors did previously (Suleman and Venkaya, 1995; Correia et al., 2000), the electrical field along the thickness direction is also assumed to be constant within each layer for saving the computational amount. This may be very approximate when the piezoelectric layer is thick. Some other authors, such as Saravanos et al. (1997), Chee et al. (2000) and Lee and Saravanos (2000), used the assumption of linear distribution of electrical potential along the thickness direction within one layer. Our later numerical example shows that the assumption of the constant electrical potential within one layer is reasonable by comparing with the layerwise approach (Lee and Saravanos, 2000) and 3D FEM of ABAQUS.

The penalty terms are described as follows

$$\boldsymbol{\psi} = \mathbf{B}_\psi \mathbf{u}^e \tag{31}$$

where $\mathbf{B}_\psi$ is written into the following form

$$\mathbf{B}_\psi = [\mathbf{B}_\psi^1, \ldots, \mathbf{B}_\psi^i, \ldots, \mathbf{B}_\psi^{\text{nd}}] \tag{32}$$

and

$$\mathbf{B}_\psi^i = \begin{bmatrix} 0 & 0 & N_i & -\partial N_i/\partial x & 0 & 0 & 0 \\ 0 & 0 & N_i & 0 & -\partial N_i/\partial y & 0 & 0 \end{bmatrix} \tag{33}$$

For the penalty stiffness matrix, due to unmatching of the orders of the interpolation functions by observing Eq. (33), the reduced integration technique has been adopted to avoid the locking phenomenon caused by penalty terms. The main problem caused by the reduced integration scheme is that it may introduce the spurious modes into the elemental stiffness matrix in some cases. After checking the eigenvalues of an elemental stiffness matrix, we found that the reduced integration scheme has not introduced the spurious modes into the present elemental stiffness matrix. Therefore, it was finally adopted due to its simplicity and lower computational cost.

Finally, the system equation can be written as

$$\begin{bmatrix} \mathbf{M}_{uu} & \mathbf{0} \\ \mathbf{0} & \mathbf{0} \end{bmatrix} \begin{Bmatrix} \ddot{\mathbf{u}} \\ \ddot{\boldsymbol{\phi}} \end{Bmatrix} + \begin{bmatrix} \mathbf{K}_{uu} & \mathbf{K}_{u\phi} \\ \mathbf{K}_{\phi u} & \mathbf{K}_{\phi\phi} \end{bmatrix} \begin{Bmatrix} \mathbf{u} \\ \boldsymbol{\phi} \end{Bmatrix} = \begin{Bmatrix} \mathbf{F}_u(t) \\ \mathbf{F}_\phi(t) \end{Bmatrix} \tag{34}$$

in which the system matrices are assembled from the elemental matrices, which are expressed as

$$\mathbf{K}^e_{uu} = \mathbf{K}^e_{uk} + \mathbf{K}^e_{up} = \int_{-1}^{+1}\int_{-1}^{+1} \mathbf{B}_{\mathrm{d}}^{\mathrm{T}}\mathbf{D}_{\mathrm{c}}\mathbf{B}_{\mathrm{d}}\ \det\mathbf{J}\,\mathrm{d}\xi\,\mathrm{d}\eta + \int_{-1}^{+1}\int_{-1}^{+1}\left(\int_{-h/2}^{h/2}\mathbf{B}_{\psi}^{\mathrm{T}}\mathbf{D}_{\mathrm{p}}\mathbf{B}_{\psi}\,\mathrm{d}z\right)\det\mathbf{J}\,\mathrm{d}\xi\,\mathrm{d}\eta \tag{35a}$$

$$\mathbf{K}^e_{u\phi} = \int_{-1}^{+1}\int_{-1}^{+1} \mathbf{B}_{\mathrm{d}}^{\mathrm{T}}\bar{\mathbf{e}}^{*}\mathbf{B}_{\phi}\ \det\mathbf{J}\,\mathrm{d}\xi\,\mathrm{d}\eta \tag{35b}$$

$$\mathbf{K}^e_{\phi\phi} = \int_{-1}^{+1}\int_{-1}^{+1}\left(\int_{-h/2}^{h/2}\mathbf{B}_{\phi}^{\mathrm{T}}\mathbf{p}\mathbf{B}_{\phi}\,\mathrm{d}z\right)\det\mathbf{J}\,\mathrm{d}\xi\,\mathrm{d}\eta \tag{35c}$$

$$\mathbf{M}^e_{uu} = \int_{-1}^{+1}\int_{-1}^{+1}\left(\int_{-h/2}^{h/2}\rho\mathbf{N}^{\mathrm{T}}\mathbf{N}\,\mathrm{d}z\right)\det\mathbf{J}\,\mathrm{d}\xi\,\mathrm{d}\eta \tag{35d}$$

Two kinds of elements, i.e. four-node and nine-node elements with Lagrange interpolation functions have been made. The penalty parameters α_x and α_y are chosen as follows from our numerical experiences

$$\alpha_x = \alpha_y = \max(|\mathbf{K}^e_{uk}|_{ij}) \times (10^3\text{–}10^5) \tag{36}$$

i.e. 10^3–10^5 times the maximum of the absolute value of entries of the matrix $\mathbf{K}^e_{uk}$ as shown in Eq. (35a).

In practice, voltage may also be specified as input to the actuators. The electric charge at the sensors $\mathbf{F}_{\phi}$ should remain constant with time (practically open-circuit conditions) and is assumed equal to zero. As a general condensation procedure, the final equation can be cast into the following form

$$\mathbf{M}_{uu}\ddot{\mathbf{u}} + \mathbf{K}^{*}\mathbf{u} = \mathbf{F}_{u} - \mathbf{F}_{\mathrm{A}} \tag{37}$$

where $\mathbf{K}^{*}$ and actuator force vector $\mathbf{F}_{\mathrm{A}}$ can be written as

$$\mathbf{K}^{*} = \mathbf{K}_{uu} - \mathbf{K}_{u\phi}\mathbf{K}^{-1}_{\phi\phi}\mathbf{K}_{\phi u}, \qquad \mathbf{F}_{\mathrm{A}} = \mathbf{K}_{u\phi}\boldsymbol{\phi}_{\mathrm{A}} \tag{38}$$

The electric potential of sensors due to deformation can be obtained as

$$\boldsymbol{\phi}_{\mathrm{S}} = -\mathbf{K}^{-1}_{\phi\phi}\mathbf{K}_{\phi u}\mathbf{u} \tag{39}$$

Further inspection of Eq. (37) reveals that the "induced-strain" approaches, in the presence of sensors, neglect the coupling effects on both the stiffness and the induced piezoelectric force. This may lead to some different results as discussed in the following numerical examples. The above dynamic system can be solved to obtain either the modal characteristics, or the forced frequency response or the transient response of the piezoelectric composite laminates.

3. Verifications

3.1. Piezoelectric bimorph beam

A numerical application has been used to validate the developed numerical models both as an actuator and a sensing mechanism, which is based on an experiment (Tzou and Tseng, 1990) and analytical results (Suleman and Venkayya, 1995; Correia et al., 2000). The experiment consists of a cantilevered piezoelectric bimorph beam with two PVDF layers bonded together and polarized in opposite directions with dimensions indicated in Fig. 1. The mechanical and piezoelectric properties of the PVDF used are: $E_{11} = E_{22} = E_{33} = 2$ GPa, $G_{12} = G_{13} = G_{23} = 1$ GPa, $v_{12} = v_{23} = v_{13} = 0.0$, $e_{31} = e_{32} = 0.0460$ C/m^2, and $p_{33} = 0.1062 \times 10^{-9}$ F/m. The e_{33} coefficient in all models is assumed to be zero.

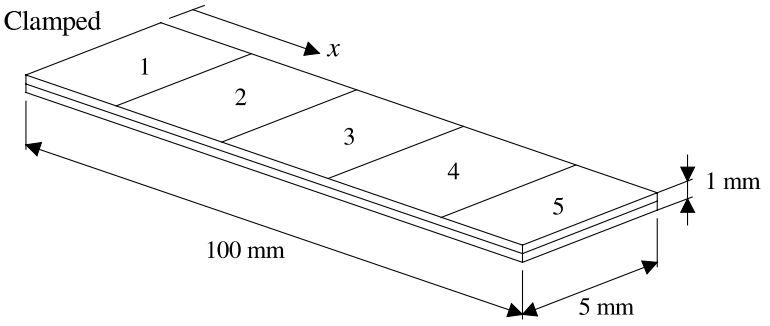

Fig. 1. Piezoelectric bimorph beam.

Table 1
Comparison of deflections induced by actuators

Location x (mm)	Deflections (10^{-7} m)				
	20	40	60	80	100
Present (nine-node element)	0.139	0.553	1.24	2.21	3.45
Present (four-node element)	0.139	0.553	1.24	2.21	3.45
Theory (Tzou and Tseng (1990))	0.138	0.552	1.24	2.21	3.45
Plate FE (11 DOFs) (Correia et al. (2000))	0.138	0.552	1.24	2.21	3.45
Plate FE (9 DOFs) (Correia et al. (2000))	0.138	0.552	1.24	2.21	3.45
Shell FE (FDST) (Tzou and Ye (1996))	0.132	0.528	1.19	2.11	3.30
Plate FE (FDST) (Suleman and Venkaya (1995))	0.14	0.55	1.24	2.21	3.45
Analytical (Correia et al. (2000))	0.13	0.51	1.14	2.02	3.16
Experimental (Tzou and Tseng (1990))	–	–	–	–	3.15

First, the beam is directly discretized into five equal nine-node plate elements in order to compare with alternative results. Also, 20 equal four-node plate elements are adopted in the present computation. When piezoelectric material is used as an actuator with an electric potential of 1 V, the deflections produced are shown in Table 1. For comparison, the results obtained from two nine-node plate elements (Correia et al., 2000) using a higher-order theory (with 11 or 9 degrees of freedom at one node, respectively), the results of the shell and plate element based on the first-order shear deformation theory, the results of theoretical solution and experimental results are also employed. From this table, it can be found that the present results are in very good agreement with other results. Also, for this example with simple deformation, the present four-node element can yield the almost same results with the nine-node element. In the following all numerical examples, only results of the nine-node element are illustrated for simplicity.

The sensing voltage distribution of the bimorph beam for a prescribed deflection is also analyzed. The voltage distribution for an imposed tip deflection of 10 mm is given in Table 2. It can be observed a good agreement between the present element voltages with the alternative solutions. The slightly lower sensed voltages in the nine-node element with 11 degrees of freedom (Correia et al., 2000) can also be identified. Furthermore, for two finite element meshes with 5 and 20 elements, the sensed element voltages along the beam obtained from the present element and those of the nine-node element (9 degrees of freedom at one node) of Correia et al. are shown in Fig. 2.

Table 2
Comparison of sensory voltages induced a prescribed tip deflection

Element number	Sensed voltage (V)				
	1	2	3	4	5
Present (nine-node element)	290	226	161	97	32.0
Plate FE (11 DOFs) (Correia et al. (2000))	276	214	153	92	32.0
Plate FE (9 DOFs) (Correia et al. (2000))	290	226	161	97	32.0
Plate FE (FDST) (Suleman and Venkaya (1995))	290	–	–	–	–

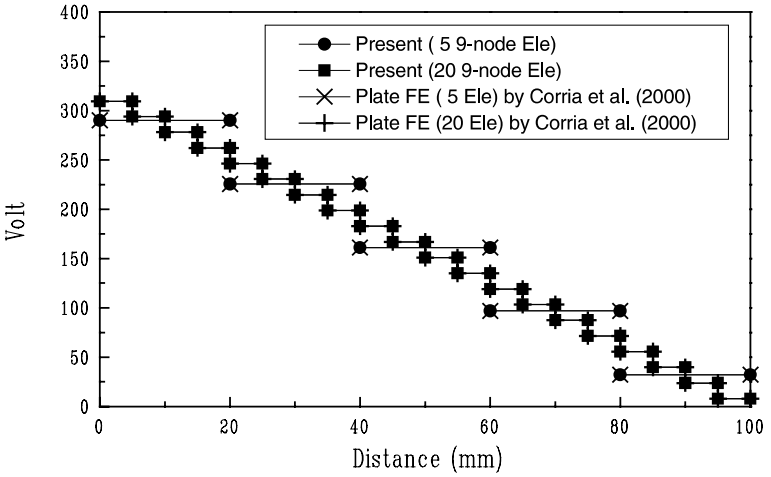

Fig. 2. Comparison of sensed element voltages for tip deflection of 10 mm.

3.2. Clamped plate with piezoelectric ceramics under thermal loading

The third example is taken from the work (Lee and Saravanos, 2000). The clamped carbon/epoxy plate with a thin piezoelectric upper layer is shown in Fig. 3, which is under uniform 50°C thermal loading. The carbon/epoxy portion consists of eight 0° plies and dimensions are shown in Fig. 3. The material properties of carbon/epoxy are listed as: $E_{11} = 142.0$ GPa, $E_{22} = 10.3$ GPa, $G_{12} = G_{13} = 7.2$ GPa, $G_{23} = 4.29$ GPa, $v_{12} = 0.27$, $\alpha_{11} = -0.9$ (μm/m°C), and $\alpha_{22} = 27.0$ (μm/m°C), where α is the thermal expansion coefficient. The material properties of the piezoceramic are: $E_{11} = 69.0$ GPa, $E_{22} = 69.0$ GPa, $G_{12} = G_{13} = G_{23} = 26.5$ GPa, $v_{12} = v_{13} = v_{23} = 0.30$, $\alpha_{11} = \alpha_{22} = 1.2$ (μm/m°C), $p_{33} = 0.1062 \times 10^{-9}$ F/m, $d_{31} = -154.0$ pm/V and $d_{32} = 0.0$ pm/V.

When the piezoelectric is used as an actuator, the centerline deflections ($y/b = 0.5$) are shown in Fig. 4. For comparison, the results of the shell and plate elements based on the layerwise theory (Lee and Saravanos, 2000) and the results of the continuum element obtained from MSC/ABAQUS commercial software have been employed. In Fig. 4, the normalized electric potential is $\phi^* = \phi \times d_{31} \times 10^5/h$ and the normalized deflection is: $w^* = 100 \times w/h$, respectively, where h is the total thickness of the plate. The finite element mesh is the same with that of Lee and Saravanos's shell element, i.e. 10×5, where 10 equal divisions were used along the plate length direction. The mesh of Lee and Saravanos's plate element is 20×10. From this figure, it can be found that the present results agree with other three kinds of results very well for the different kinds of applied electric potentials although the plate is relatively thick.

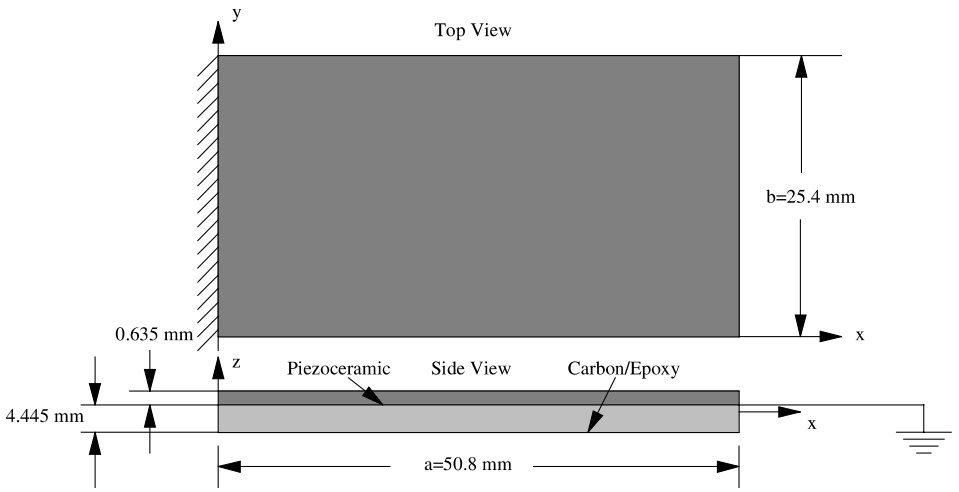

Fig. 3. Geometry of a clamped plate with an attached piezoelectric layer.

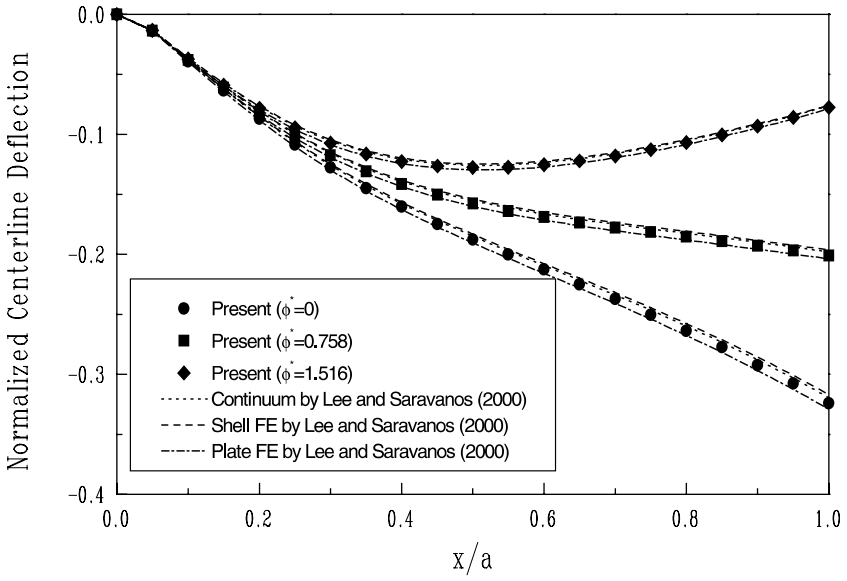

Fig. 4. Comparison of displacements under active electric potentials of a clamped plate.

When the piezoelectric layer is used as a sensor, the centerline deflections are shown in Fig. 6. Also, the generated electric potentials due to thermal deformation in this case are shown in Fig. 6. To reflect the severe variation of the electric potential near the clamped end, the element size is changed to be quite small near the fixed end. From these two figures, it can be observed that the present results are very near other three results. From Fig. 6, by comparing with the maximum electric potential at the fixed end given by the continuum element of MSC/ABAQUS, the present FEM scheme can yield the closer results than those of the shell and plate elements (Lee and Saravanos, 2000). Further, comparing Fig. 5 with Fig. 4, it can be found that the deflection becomes a little lower due to the transformation of mechanical energy to electric energy.

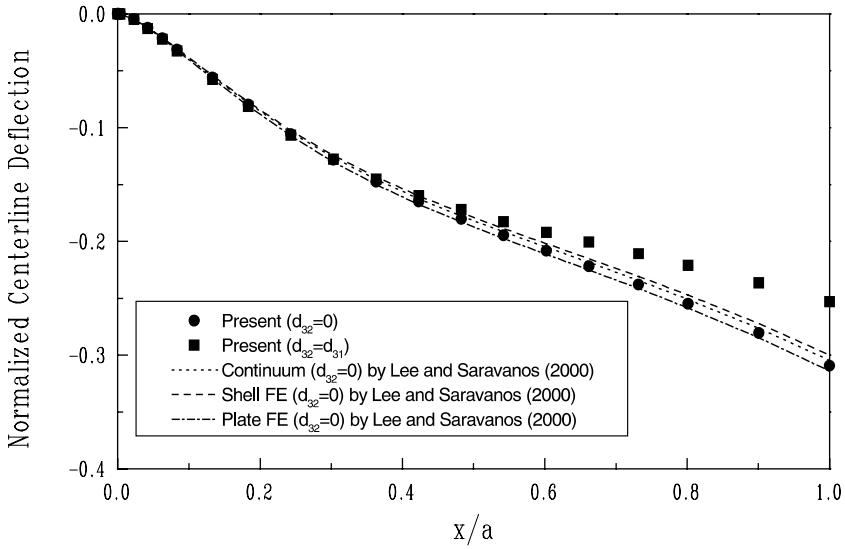

Fig. 5. Comparison of thermally induced sensory displacements of a clamped plate.

In the above computation, d_{32} is assumed to be zero. When d_{32} is set to be equal to d_{31}, the deflection results and the electrical potentials of sensors on the centerline are also shown in Figs. 5 and 6. From these figures, when d_{32} changes from zero to the value of d_{31}, it can be found that the maximum deflection of plate becomes smaller, and the electrical potentials of sensors become higher. The reason is that more mechanical energy has been exchanged into the electrical energy. The deformation configuration of plate is shown in Fig. 7. Investigation of this figure reveals that there is severe bending deformation along the y-axis besides that along the x-axis due to the low bending stiffness (0° ply) in the y-axis direction. Then when d_{32} is not

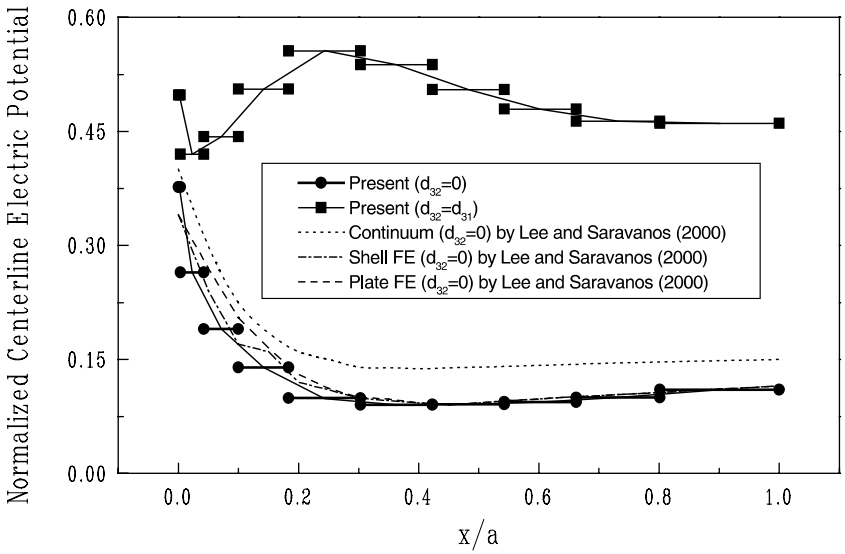

Fig. 6. Comparison of thermally induced sensory electric potentials of a clamped plate.

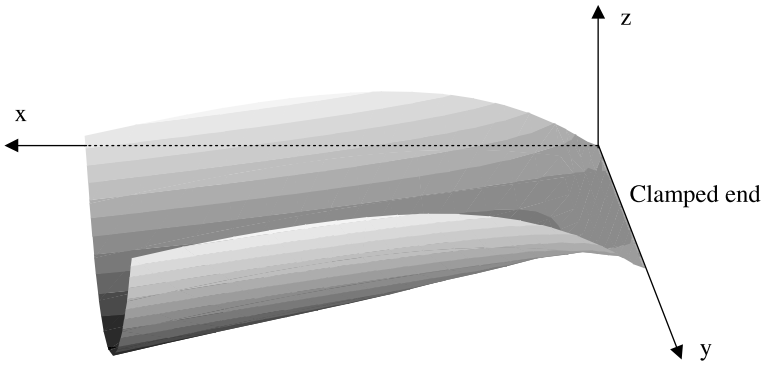

Fig. 7. Deformation configuration of a clamped plate.

equal to zero, the bending deformation in the y-axis direction can lead to the increase of the electrical potential of sensors, consequently the mechanical energy becomes lower further and the deformation of the plate decreases. In this case, the "induced-strain" approaches, which neglect the coupling of mechanical and electric effects, may lead to the larger deflection of plate due to no loss of the mechanical energy, and then the resulted electrical potentials from the larger deflection may also be higher.

3.3. Static and dynamic (FRF) piezoelectric responses

The work (Keilers and Chang, 1995) has also been employed for checking the present method. A clamped beam with actuator and sensor near the fixed end is analyzed. The dimensions of the beam of $[0/+45/-45]_s$ are shown in Fig. 8. The materials constants of T300/976 composite are: $E_{11} = 150.0$ GPa, $E_{22} = 9.0$ GPa, $G_{12} = G_{13} = 7.1$ GPa, $G_{23} = 2.5$ GPa, $v_{12} = 0.3$ and $\rho = 1600$ kg/m^3. The thickness of one lamina and the piezoelectrics is 0.127 mm. The material properties of the piezoelectric layer are: $E_{11} = 63.0$ GPa, $E_{22} = 63.0$ GPa, $G_{12} = G_{13} = G_{23} = 24.2$ GPa, $v_{12} = v_{13} = v_{23} = 0.30$, $\rho = 7600$ kg/m^3, $p_{33} = 19.5$ nF/m and $d_{31} = d_{32} = -170.0$ pm/V.

Twenty nine-node elements along the length direction of the beam are used in which three elements are used for the actuator and sensor portion. The results of the potential of sensors under the static actuator load are first validated as shown in Fig. 9. Investigation of Fig. 9 reveals that there is a linear relationship between the applied actuator voltage and the produced sensor potential. Also, compared with the

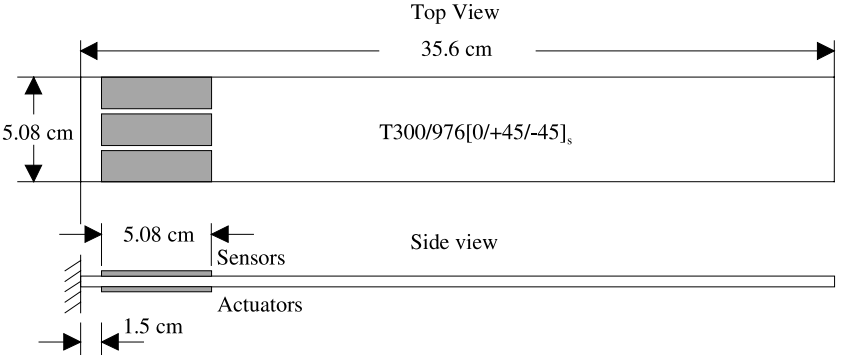

Fig. 8. Geometry of a clamped beam with surface attached actuators and sensors.

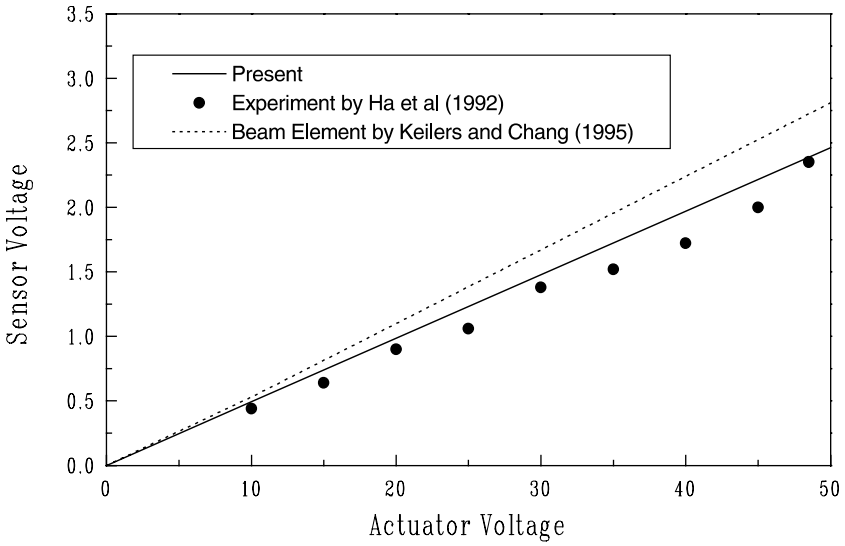

Fig. 9. Comparison of induced sensor voltages due to static actuator voltages.

experimental results, the present FEM model, i.e. a fully linear model, can yield more accurate results than those of the beam element (Keilers and Chang, 1995). It is obvious that the plate theory is a more detailed model than a 2D beam model and consequently produces more detailed results.

When the actuators is applied the harmonic dynamic input, i.e. $\phi_A \sin(\omega t)$, the produced frequency response function of the sensor potential ϕ_S are also computed. To reduce the computational amount of the analysis of frequency response function, here the modal superposition technique has been adopted. In the present example, the assumption of no damping is employed. Furthermore, for computing the FRF, the first 60-order modal data of the FEM model are employed in the modal superposition technique in FRF

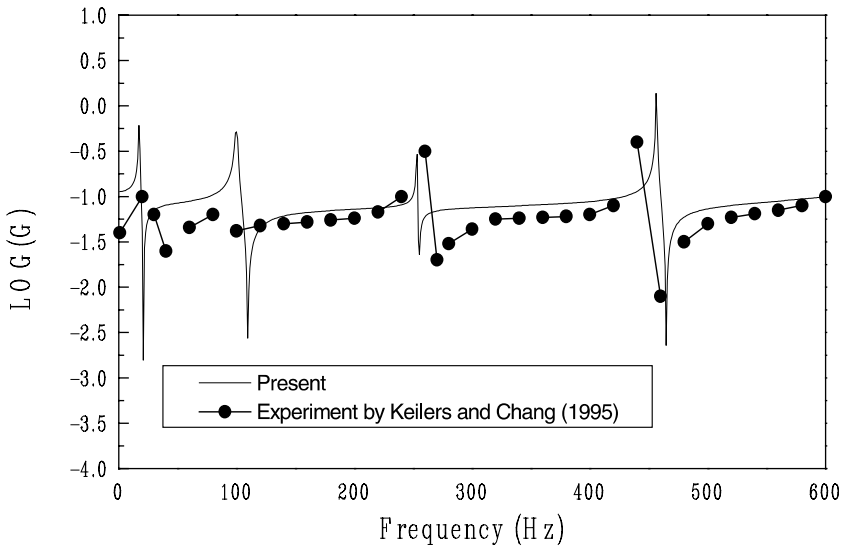

Fig. 10. Comparison of induced sensor voltages due to harmonic actuator voltages.

analysis. The amplitude (normal) of the complex FRF of ϕ_S are normalized by the actuator input as follows: $G = |\phi_S|/|\phi_A|$. The FRF of sensor potentials of the first four bending modes are shown in Fig. 10 by comparing with the experimental results of Keilers and Chang (1995). From this figure, the reasonable present results can be identified.

4. Conclusions

The development of mathematical models to describe the static or dynamic behavior of composite adaptive structures with piezoelectric actuators and sensors has been presented. The present research has fulfilled the following targets: first, based on a simple higher-order plate theory, a C^0-type finite element has been constructed through the introduction of two artificial variables and the penalty function method; second, the coupling effects of the mechanical and electric fields have been included starting from the general variational framework. Good correlations have been obtained between the developed finite element model and alternative solutions or experimental results in previous researches for various problems. The computational accuracy and efficiency of the present model have been illustrated. The application of the present FEM model for our other researches, e.g. the damage identification, will be reported in the near future.

Acknowledgements

The present authors wish to express their sincere gratefulness to Dr. H.-J. Lee and Dr. D.A. Saravanos at NASA Glenn Research Center for providing the detailed information about their researches and some invaluable comments on the present work.

References

Bisegna, P., Maceri, F., 1996. An exact three-dimensional solution for simply supported rectangular piezoelectric plates. Journal of Applied Mechanics 63, 628–638.

Chattopadhyay, A., Seeley, C.E., 1997. A higher order theory for modeling composite laminates with induced strain actuators. Composites Part B 288, 243–253.

Chee, C., Tong, L., Steven, G., 2000. A mixed model for adaptive composite plates with piezoelectric for anisotropic actuation. Computers and Structures 77, 253–268.

Correia, F.V.M., Gomes, M.A.A., Suleman, A., et al., 2000. Modelling and design of adaptive composite structures. Computer Methods in Applied Mechanics and Engineering 185, 325–346.

Crawley, E.F., Lazarus, K.B., 1989. Induced strain actuation of composite plates. AIAA Paper 89-1326-CP, 30th AIAA Structural Dynamics and Materials Conference, Mobile, Alabama.

Gaudenzi, P., 1998. Exact higher order solutions for a simple adaptive structure. International Journal of Solids and Structures 35, 26–27.

Ha, S.K., Keilers, C.H., Chang, F.K., 1992. Finite element analysis of composite structures containing distributed piezoceramic sensors and actuators. AIAA Journal 30 (3), 772–780.

Heyliger, P.R., Saravanos, D.A., 1995. Exact free-vibration analysis of laminated plates with embedded piezoelectric layers. Journal of Acoustical Society of America 98, 1547–1557.

Jemielita, G., 1975. Techniczna teoria plyt sredniej grubbosci (Technical theory of plates with moderate thickness). Rozprawy Inzynierskie (Engng. Trans.), Polska Akademia Nauk 23, 483–499.

Keilers, C.H., Chang, F.K., 1995. Identification delamination in composite beams using built-in piezoelectrics: Part I – Experimental and analysis. Journal of Intelligent Material Systems and Structures 6, 649–663.

Kim, J., Varadan, V., Varadan, K., 1997. Finite element modeling of structures including piezoelectric active devices. International Journal of Numerical Methods in Engineering 40, 817–832.

Lee, H.-J., Saravanos, D.A., 1997. Generalized finite element formulation for smart multilayered thermal piezoelectric composite plates. International Journal of Solids and Structures 34, 3355–3371.

Lee, H.-J., Saravanos, D.A., 2000. A mixed multi-field finite element formulation for thermopiezoelectric composite shells. International Journal of Solids and Structures 37, 4949–4967.

Lo, K.H., Christensen, R.M., Wu, E.M., 1977. A high order theory of plate deformation: Parts I and II: homogeneous plates. Journal of Applied Mechanics 44, 663–676.

Mollenhauer, D.H., Griffen, O.H., Jr., 1994. Induced strain of actuation of surface bonded piezoelectric patches: a numerical and experimental study. Journal of Intelligent Material Systems and Structures 5, 335–362.

Murthy, M.V.V., 1981. An improved transverse shear deformation theory for laminated anisotropic plates. NASA Technical Paper 1903, 1–37.

Reddy, J.N., 1984. A simple higher-order theory for laminated composite plates. Journal of Applied Mechanics 51, 745–752.

Robbins, D.H., Reddy, J.N., 1991. Analysis of piezoelectrically actuated beams using a layerwise displacement theory. Composite Structures 41 (2), 265–279.

Saravanos, D.A., Heyliger, P.R., Hopkins, D.A., 1997. Layerwise mechanics and finite element for the dynamic analysis of piezoelectric composite plates. International Journal of Solids and Structures 34 (3), 359–378.

Seeley, C.E., Chattopadhyay, A., 1999. Modeling of adaptive composites including debonding. International Journal of Solids and Structures 36, 1823–1843.

Shu, J.Y., King, W.E., Fleck, N.A., 1999. Finite elements for materials with strain gradient effects. International Journal of Numerical Methods in Engineering 44, 373–391.

Suleman, A., Venkaya, V.B., 1995. A simple finite element formulation for a laminated composite plate with piezoelectric layers. Journal of Intelligent Material Systems and Structures 6, 776–782.

Tzou, H.S., Tseng, C.I., 1990. Distributed piezoelectric sensor/actuator design for dynamic measurement/control of distributed parameter systems: a piezoelectric finite element approach. Journal of Sound and Vibration 138 (1), 17–34.

Tzou, H.S., Ye, R., 1996. Analysis of piezoelectric structures with laminated piezoelectric triangle shell elements. AIAA Journal 34 (1), 110–115.

Vlasov, B.F., 1957. Ob uravnieniakh izgiba plastinok (On equations of bending of plates). Dokla Ak. Nauk Azerbeijanskoi SSR °3, 933–959 (in Russian).